Using long-term water balances to parameterize surface conductances and calculate evaporation at 0.05° spatial resolution

Yongqiang Zhang,[1] Ray Leuning,[2] Lindsay B. Hutley,[3] Jason Beringer,[4] Ian McHugh,[4] and Jeffrey P. Walker[5]

Received 30 September 2009; revised 27 November 2009; accepted 15 December 2009; published 11 May 2010.

[1] Evaporation from the land surface, averaged over successive 8 day intervals and at 0.05° (~5 km) spatial resolution, was calculated using the Penman-Monteith (PM) energy balance equation, gridded meteorology, and a simple biophysical model for surface conductance. This conductance is a function of evaporation from the soil surface, leaf area index, absorbed photosynthetically active radiation, atmospheric water vapor pressure deficit, and maximum stomatal conductance (g_{sx}). The novelty of this paper is the use of a "Budyko-curve" hydrometeorological model to estimate mean annual evaporation rates and hence a unique value of g_{sx} for each grid cell across the Australian continent. First, the hydrometeorological model was calibrated using long-term water balances from 285 gauged catchments. Second, gridded meteorological data were used with the calibrated hydrometeorological model to estimate mean annual average evaporation ($\overline{E}$) for each grid cell. Third, the value of g_{sx} for each cell was adjusted to equate $\overline{E}$ calculated using the PM equation with $\overline{E}$ from the hydrometeorological model. This closes the annual water balance but allows the PM equation to provide a finer temporal resolution for evaporation than is possible with an annual water balance model. There was satisfactory agreement ($0.49 < R^2 < 0.80$) between 8 day average evaporation rates obtained using remotely sensed leaf area indices, the parameterized PM equation, and observations of actual evaporation at four Australian eddy covariance flux sites for the period 2000–2008. The evaporation product can be used for hydrological model calibration to improve runoff prediction studies in ungauged catchments.

Citation: Zhang, Y., R. Leuning, L. B. Hutley, J. Beringer, I. McHugh, and J. P. Walker (2010), Using long-term water balances to parameterize surface conductances and calculate evaporation at 0.05° spatial resolution, *Water Resour. Res.*, *46*, W05512, doi:10.1029/2009WR008716.

1. Introduction

[2] A fundamental problem in modeling evaporation (E) from land surfaces, comparable with uncertainties and errors in model structure, forcing information, and validation data, is determining the spatial variation of key model parameters. Here we address this issue in the context of evaluating the parameters needed to estimate actual evaporation at 0.05° spatial resolution and 8 day temporal resolution using the Penman-Monteith (PM) energy balance equation [*Monteith*, 1964]. Successful implementation of this equation requires knowledge of the available energy, atmospheric humidity deficit, and the aerodynamic conductance for each pixel, all of which can be calculated from gridded meteorological fields, remotely sensed surface albedos, and vegetation cover types. A more difficult problem is evaluating the spatial and temporal variation in surface conductance (G_s). This was done by *Cleugh et al.* [2007] by assuming that G_s is a linear function of leaf area index (LAI), obtained remotely from the Moderate Resolution Imaging Spectrometer (MODIS) on the polar-orbiting Terra satellite [*Myneni et al.*, 2002]. Spatial and temporal variations in LAI thus translate directly into variations in G_s. *Mu et al.* [2007] improved the model of *Cleugh et al.* [2007] by partitioning total E into transpiration from the canopy and evaporation from the soil. Canopy conductance (G_c) needed to calculate transpiration was estimated by *Mu et al.* [2007] as a constant times LAI, multiplied by two functions to account for the response of stomata to temperature and humidity deficit of the air. A map of vegetation type combined with a biome properties lookup table was used to allocate parameters for these functions. Of necessity, this approach assumes that the model parameters are unique for each vegetation type.

[3] In a further development of the PM approach, *Leuning et al.* [2008] replaced the earlier empirical models for G_s and G_c with a biophysical model for canopy conductance that

[1]CSIRO Water for a Healthy Country National Research Flagship, CSIRO Land and Water, Canberra, ACT, Australia.
[2]CSIRO Marine and Atmospheric Research, Canberra, ACT, Australia.
[3]School of Environmental and Life Sciences, Charles Darwin University, Darwin, Northern Territory, Australia.
[4]School of Geography and Environmental Science, Monash University, Clayton, Victoria, Australia.
[5]Department of Civil and Environmental Engineering, University of Melbourne, Melbourne, Victoria, Australia.

0043-1397/10/2009WR008716

accounts for sensitivity of stomatal conductance to sunlight and to atmospheric humidity deficit. Evaporation from the soil is estimated using a simple extra term. *Leuning et al.* [2008] used data from 15 flux stations distributed globally to show that the combined PM equation and model for G_c (denoted the PML model) requires precise knowledge of only two parameters, g_{sx}, the maximum stomatal conductance of leaves, and f, the ratio of actual to potential evaporation at the soil surface. Other model parameters can be held constant without significant loss of precision in calculating E. *Zhang et al.* [2008] used the PML model to determine 8 day mean evaporation rates (E_{PML}) across the Murray Darling Basin (MDB, Australia) at 1 km spatial resolution. To do so, they optimized values of g_{sx} and f for three rainfall zones in the MDB by minimizing the difference between mean annual $\overline{E}_{\mathrm{PML}}$ and $\overline{E}_{\mathrm{WB}}$, evaporation rates calculated from the annual water balances (precipitation minus runoff) of 120 gauged catchments (symbols with an overbar refer to annual means, and those without them refer to shorter periods). Annual evaporation and runoff calculated using the PML model had a root-mean-square error (RMSE) of <80 mm/yr in semihumid and humid regions where significant runoff was observed. However, the model overestimated evaporation in some semiarid and arid catchments because there were no water balance constraints when applying the PML model. These results suggest that it is necessary to further improve performance of the PML model by using water balances to constrain acceptable values of g_{sx} and f and through better knowledge of their spatial distribution. Obtaining valid, spatially explicit parameter values remains a challenge.

[4] In this paper the spatial variability in f is accounted for by calculating it as a variable for each grid cell. To estimate the spatial distribution of g_{sx} we present a novel approach that uses a map of mean annual evaporation for Australia derived from a calibrated water balance model. As a first step in our analysis, $\overline{E}_{\mathrm{WB}}$ calculated from water balances of 285 gauged, unregulated catchments over the period of 2000–2005 were used to estimate the single parameter in the rational function of *Fu* [1981]. This is one of the classic "Budyko-curve" models [*Budyko*, 1958] which relates the actual evaporation index ($\overline{E}/\overline{P}$) to the aridity index ($\overline{E}_p/\overline{P}$), where $\overline{E}$, $\overline{E}_p$, and $\overline{P}$ are mean annual actual and potential evaporation and precipitation, respectively. The calibrated Fu model was next combined with gridded meteorological data to generate a map of mean annual evaporation ($\overline{E}_{\mathrm{Fu}}$) at 0.05° (~5 km) resolution across Australia for the period 2000–2005. The spatially distributed values of $\overline{E}_{\mathrm{Fu}}$ were then used to estimate g_{sx} for each pixel by adjusting g_{sx} to force $\overline{E}_{\mathrm{Fu}} = \overline{E}_{\mathrm{PML}}$ for each pixel. Finally, 8 day actual evaporation rates for each grid cell from 2000 to 2008 were estimated using the PML model with the best estimate of g_{sx}, remotely sensed albedo and land cover data, 8 day average meteorology, and 8 day MODIS updates of LAI. This approach ensures closure of the annual water balance for each pixel through matching of $\overline{E}_{\mathrm{Fu}}$ and $\overline{E}_{\mathrm{PML}}$ while allowing a fine temporal resolution using E_{PML}.

2. Theory

2.1. Daily Evaporation and Energy Balance

[5] *Leuning et al.* [2008] showed that the total flux of latent heat λE (MJ/m^2/d) associated with the sum of transpiration from the plant canopy (λE_c, MJ/m^2/d) and evaporation from the soil (λE_s, MJ/m^2/d) can be written as

$$\lambda E = \frac{\varepsilon A_c + (\rho c_p/\gamma) D_a G_a}{\varepsilon + 1 + G_a/G_c} + \frac{f\varepsilon A_s}{\varepsilon + 1}, \tag{1}$$

The first term on the right uses the PM equation [*Monteith*, 1964] to express λE_c in terms of the net energy absorbed by the canopy (A_c, MJ/m^2/d), the water vapor pressure deficit of the air at a reference height above the canopy (D_a, kPa), the aerodynamic conductance (G_a, MJ/m^2/d), and the canopy conductance (G_c, m/s). Here λ is the latent heat of evaporation (MJ/kg), $\varepsilon = s/\gamma$, in which γ is the psychrometric constant (kPa/°C), and $s = de^*/dt$, the slope of the curve relating saturation water vapor pressure to temperature (kPa/°C), ρ is the density of air (kg/mP^3), and c_p is the specific heat of air at constant pressure (J/kg/°C).

[6] The net energy absorbed by the vegetation canopy plus soil (A) (MJ/m^2/d) is partitioned into $A_c = (1 - \tau)A$ and $A_s = \tau A$, respectively, where $\tau = \exp(-k_A \mathrm{LAI})$, and k_A is the extinction coefficient for net radiation (comprising visible, near-infrared, and thermal radiation). The second term of equation (1) is used to estimate λE_s as a (variable) fraction f of the equilibrium evaporation rate, $\varepsilon A_s/(1 + \varepsilon)$.

[7] Estimating the spatial and temporal variation in λE using equation (1) requires knowledge of A_c and A_s. These were calculated using LAI and surface albedo from MODIS remote sensing and gridded, daily average fields of solar radiation. Daytime averages of temperatures, humidities, and wind speeds were used to calculate D_a and G_a. Equation (1) also requires the space-time distributions of the soil evaporation coefficient f and canopy conductance G_c.

[8] The coefficient f varies from $f = 1$ when the soil surface is wet to $f = 0$ when it is dry, but due to a lack of seasonally varying soil moisture data, f was earlier treated as a fixed parameter to be estimated using either flux station data [*Leuning et al.*, 2008] or mean annual water balances of gauged catchments [*Zhang et al.*, 2008]. Analysis by *Leuning et al.* [2008] showed that the PML model is not sensitive to uncertainties in f when LAI > 2.5 because soil evaporation is a then a small fraction of the total. This is not the case for sparse canopies, and it is then unsatisfactory to assume that f is a constant. In the absence of any observed space-time distributions of soil moisture in this study, variation in f for each grid cell was estimated using

$$f = \min\left(\frac{\sum_{n=-N}^{N} P_n}{\sum_{n=-N}^{N} E_{\mathrm{eq},s,n}}, 1 \right), \tag{2}$$

where P_n is precipitation (mm/d) for each 8 day period n and $E_{\mathrm{eq},s,n} = \mathrm{A}_{s,n}(\varepsilon/\lambda)/(\varepsilon + 1)$ is the average equilibrium evaporation rate (mm/d) according to the energy available at the soil surface for that period. We set $N = 4$, indicating that P_n and $E_{\mathrm{eq},s,n}$ were summed over four periods prior and four periods after the current one. This smoothing allows for gradual changes in surface soil moisture and avoids the problem of f switching rapidly from $f = 0$, if

there has been no rainfall in a given 8 day period, to $f = 1$ during periods of rain.

[9] To estimate G_c, *Leuning et al.* [2008] used the following relatively simple model developed by *Saugier and Katerji* [1991], *Dolman et al.* [1991], and *Kelliher et al.* [1995] for G_c as a function of visible radiation and leaf area index and modified by *Isaac et al.* [2004] to account for the influence of atmospheric humidity deficit on G_c:

$$G_c = \frac{g_{sx}}{k_Q}\ln\left[\frac{Q_h + Q_{50}}{Q_h \exp(-k_Q \mathrm{LAI}) + Q_{50}}\right]\left[\frac{1}{1 + D_a/D_{50}}\right]. \quad (3)$$

Here g_{sx} is the maximum stomatal conductance (m/s) of leaves at the top of the canopy, k_Q is the extinction coefficient for visible radiation, and Q_h is the flux density of visible radiation at the top of the canopy (MJ/m^2/d). The parameters Q_{50} and D_{50} are the visible radiation flux (MJ/m^2/d) and the humidity deficit (kPa), respectively, at which stomatal conductance is half its maximum value. The PML model for G_c contains five parameters, but *Leuning et al.* [2008] showed that the model could be simplified considerably by using fixed values for four parameters ($k_Q = k_A = 0.6$, $Q_{50} = 30$ W/m^2, and $D_{50} = 0.7$ kPa), with variable g_{sx} to calculate G_c and then λE_c from equation (1). This approach yielded values of λE_c very similar to those obtained when all five parameters were optimized using data from each of 15 flux station sites covering a wide range in climate and vegetation types globally. Calculation of the spatial and temporal variation of G_c thus requires g_{sx} (currently unknown), incoming visible radiation and atmospheric humidity deficit obtained from gridded meteorological data, and LAI from MODIS remote sensing.

[10] It is worth noting that G_c as defined by equation (3) can vary on time scales ranging from minutes to years, through the diurnal to seasonal variations in Q_h and D_a and through the weekly to annual variations in LAI. These will affect E indirectly through changes in G_c, whereas variations in A_c, A_s, D_a, and G_a will affect E directly at all time scales (equation (1)). Soil moisture content also affects G_c, but there is no explicit dependence between the two in equation (3) because we want to apply this equation using remotely sensed and gridded meteorological data only. However, an indirect dependence of G_c on soil moisture occurs through the landscape-scale adjustment of D_a and LAI to long-term soil water availability.

2.2. Long-Term Evaporation and Water Balance

[11] In pioneering work, *Budyko* [1958, 1974] noted that mean annual evaporation from a catchment is determined by a balance between the energy available for evaporation and the amount of available water. The Budyko curve expresses the evaporation index ($\overline{E}/\overline{P}$) as a function of the aridity index ($\overline{E}_p/\overline{P}$), where $\overline{E}_p$ is mean annual potential evaporation (mm/yr). In this paper we use a variant of the Budyko curve developed by *Fu* [1981] that is given by

$$\frac{\overline{E}_{\mathrm{Fu},i}}{\overline{P}_i} = 1 + \frac{\overline{E}_{pi}}{\overline{P}_i} - \left[1 + \left(\frac{\overline{E}_{pi}}{\overline{P}_i}\right)^{\alpha}\right]^{1/\alpha}, \quad (4)$$

where $\overline{E}_{\mathrm{Fu},i}$ is the mean annual evaporation for $i = 1,\ldots, M$ catchments, α is a parameter, and $\overline{E}_{pi}$ is the mean annual potential evaporation for catchment i. $\overline{E}_{pi}$ was calculated by averaging daily Priestley-Taylor potential evaporation:

$$\overline{E}_{pi} = \alpha_{\mathrm{PT}} \sum_{1}^{365} \frac{\varepsilon A_i}{\varepsilon + 1}, \quad (5)$$

where $\alpha_{PT} = 1.26$ [*Priestley and Taylor*, 1972]. Daytime-averages of ε and A_i for a given catchment are used in the summation. Mean annual evaporation for water bodies was calculated using $\overline{E}_{pi}$.

[12] The general pattern search method in Matlab (http://www.mathworks.com/access/helpdesk_r13/help/pdf_doc/gads/gads_tb.pdf) was used to obtain an optimal value for α by fitting equation (4) to observed $\overline{E}_i$, calculated as $\overline{E}_i = \overline{P}_i - \overline{Q}_i$, the residual between mean annual precipitation ($\overline{P}_i$) and runoff ($\overline{Q}_i$) for all 285 gauged catchments. The Fu model with the optimized value of α was then combined with gridded meteorological data to produce a map of $\overline{E}_{\mathrm{Fu}}$ for each 0.05° grid cell across Australia. The nonlinear least squares regression in Matlab (http://www.mathworks.com/access/helpdesk/help/pdf_doc/stats/stats.pdf) was then used to estimate a unique value of g_{sx} for each grid cell by adjusting g_{sx} to ensure that $\overline{E}_{\mathrm{Fu}} = \overline{E}_{\mathrm{PML}}$ for that cell. The PML model has the advantage of providing evaporation rates at a fine temporal resolution, while our optimization scheme ensures closure of the annual water balance. Another advantage of the optimization is that, through equation (3), any errors in the remotely sensed values of LAI will lead to compensating errors in estimates of g_{sx}.

3. Data

[13] Data used for this study include 8 day MODIS/Terra LAI, 8 day MODIS/Terra albedo, annual MODIS/Terra land cover classifications, daily meteorology, a digital elevation model (DEM), and daily streamflows. Precipitation and streamflow data for 285 catchments from 2000 to 2005 were first used to calibrate the Fu model (note that streamflow data for these catchments were only available until 2005). Gridded meteorological data were next used to produce a map of $\overline{E}_{\mathrm{Fu}}$ and g_{sx}, which was than combined with time series of gridded meteorology and remote-sensing data to calculate 8 day E_{PML} for each grid cell across Australia from 2000 to 2008.

[14] Remotely sensed LAI data were provided by *Paget and King* [2008], who extracted the MOD15A2 (collection 5.0) data products at 1 km resolution across Australia for the period 2000–2008 from the Land Processes Distributed Active Archive Centre (LPDAAC) (http://lpdaac.usgs.gov/dataproducts.asp). Quality assessment flags in the database were used to delete all poor-quality LAI data, and these were replaced by interpolated values obtained from a piecewise cubic, Hermite interpolating polynomial [*Zhang and Wegehenkel*, 2006]. The quality-controlled LAI data for each pixel were then smoothed using the Savitzky-Golay filtering method that is widely used for filtering MODIS LAI and other remote sensing data [*Jonsson and Eklundh*, 2004; *Ruffin et al.*, 2008; *Tsai and Philpot*, 1998].

[15] The quality of MODIS-LAI data is best at LAI < 3, but the precision declines at higher values due to saturation of the reflectance signal [*Yang et al.*, 2006]. Many studies

have shown that the quality of MODIS LAI data is reasonably good for most land cover types, but for forests with high LAI, MODIS LAI is easily overestimated owing to reflectance saturation [*Cohen et al.*, 2006; *Garrigues et al.*, 2008; *Hill et al.*, 2006; *Yang et al.*, 2006].

[16] Daily meteorological data (maximum air temperature, T_{max}, minimum air temperature, T_{min}, solar radiation, R_s, vapor pressure, e, and precipitation, P) from 2000 to 2008 at 0.05° (~5 km) resolution were obtained from the SILO Data Drill of the Queensland Department of Natural Resources and Water (http://www.nrw.qld.gov.au/silo/datadrill/). The SILO data are interpolated from approximately 4600 point observations across Australia using the methods of *Jeffrey et al.* [2001]. A thin plate smoothing spline was used to interpolate daily climate variables, and ordinary kriging was used to interpolate daily and month precipitation. Cross-validated interpolation statistics for T_{max}, T_{min}, e, and P shows the mean absolute values 1.0°C, 1.4°C, 0.15 kPa, and 12.2 mm/month, respectively, indicating reasonably good data quality [*Jeffrey et al.*, 2001]. Eight day composites for T_{max}, T_{min}, R_s, e, and u were estimated from the average of the daily data according to each 8 day MODIS LAI compositing period.

[17] Gridded wind speed (u) data for 2000 to 2006 were obtained by interpolating measurements from an expanded anemometer network [*McVicar et al.*, 2008]. Wind speed data were not available for 2007–2008, so average wind speed for each pixel from 2000 to 2006 was used instead. Aerodynamic roughness lengths associated with various land cover types were used with the u data to calculate aerodynamic conductance G_a as described by *Zhang et al.* [2008]. Land cover classification data (MOD12Q1) for 2001 at 1 km resolution were obtained from the LPDAAC (http://lpdaac.usgs.gov/) (Figure 2). There are 13 land cover classes in the MOD12Q1 data set relevant to Australia: evergreen needleleaf forest, evergreen broadleaf forest, deciduous needleleaf forest, deciduous broadleaf forest, mixed forest, closed shrublands, open shrublands, woody savannas, savannas, grasslands, croplands, urban and built up, and barren.

[18] Albedo is needed to calculate the energy available for evaporation. The short-wave band (300–5000 nm) of the white-sky albedo from the 1 km resolution, 8 day MODIS MCD43B bidirectional reflectance distribution function product was used to define surface albedo [*Dilley et al.*, 2000; *Schaaf et al.*, 2002]. As for LAI, the albedo data for each pixel were quality controlled and then smoothed using the Savitzky-Golay filtering method. A DEM at 9 s resolution was provided by the Australian Surveying and Land Information Group [*Hutchinson et al.*, 2001]. The albedo and DEM data were used to calculate clear-sky solar radiation, net radiation, and then available energy for use in equation (1) (see *Zhang et al.* [2008, equations (7)–(9)]). All the DEM and remotely sensed data were resampled (spatially averaged) to the 0.05° grids used for the meteorological data.

[19] A total of 285 gauged, unregulated catchments ranging in area from 50 to 2000 km^2 (Figure 1) were selected to calculate mean annual evaporation ($\overline{E}$) for each catchment as the difference between mean annual precipitation and streamflow. The computed values of $\overline{E}$ were then used to calibrate the Fu model (equation (4)). Daily streamflow data from 2000 to 2005 were made available through the Australian Land and Water Resource Audit Project (http://www.nlwra.gov.au/) and were quality controlled. Less than 5% of data were missing after quality control for all the selected catchments, and the missing data were infilled using streamflow data observed at the nearest neighbor catchment according to the streamflow relationship between the two.

[20] Fluxes of water vapor measured at four sites (Figure 1) were compared to the 8 day variation of E_{PML} in the grid cell encompassing each flux station. These are the only Australian flux sites for which there are continuous data available for at least 1 year. The sites are (1) Tumbarumba (broadleaf evergreen forest after the International Geosphere-Biosphere Programme vegetation classification), (2) Virginia Park (open woody savanna), (3) Howard Springs (woody savanna), and (4) Dargo High Plains (grassland). Details of these flux sites are given in Table 1. Hourly average fluxes were summed over daylight hours to obtain daily E, and these were further averaged to align with the 8 day MODIS-compositing periods.

4. Calibration and Cross Validation

[21] The generalized pattern search method was used to calibrate the single parameter α in the Fu model using evaporation rates $\overline{E}_i$ derived from the catchment water balances.

[22] The objective function for the Fu model is

$$F = 1 - \mathrm{NSE} = \frac{\sum_{i=1}^{M} \left(\overline{E}_i - \overline{E}_{\mathrm{Fu},i}\right)^2}{\sum_{i=1}^{M} \left(\overline{E}_i - \overline{E}\right)^2}, \quad (6)$$

where $\overline{E}$ is the mean annual water balance evaporation across all $i = 1,\ldots, M$ catchments and $\overline{E}_{\mathrm{Fu},i}$ is calculated from equation (4). NSE is the Nash-Sutcliffe efficiency [*Nash and Sutcliffe*, 1970], which describes the degree of agreement between modeled and measured values; NSE = 1.0 indicates perfect agreement, and NSE $\leq$ 0 indicates poor agreement.

[23] The model was validated using the jackknife cross-validation method. Data from one "ungauged" catchment was left out of the optimization while data from all other catchments were used for model calibration. All 285 catchments were stepped through in this way, and the performance of the cross-validated model was tested against evaporation estimates from the water balance of every "ungauged" catchment.

5. Results and Discussion

5.1. Comparing Catchment Mean Annual Evaporation Estimates

[24] In Figure 3 the evaporation index ($\overline{E}/\overline{P}$) is plotted as a function of the aridity index ($\overline{E}_p/\overline{P}$) for all 285 gauged catchments. Despite the considerable scatter of data points around the curve of best fit for the Fu model (Figure 3a), $\overline{E}_{\mathrm{Fu}}$, calculated using a single, optimized value of $\alpha = 3.39$ explains 85% of the variance in $\overline{E}_{\mathrm{WB}}$, with an RMSE of 57.1 mm/yr and an NSE = 0.85 (Figure 3b). A jackknife cross-validation analysis yielded values of $\overline{E}_{\mathrm{Fu}}$ very similar to those obtained using the full data set, with the RMSE increasing from 57.1 to 57.4 mm and no change to the NSE.

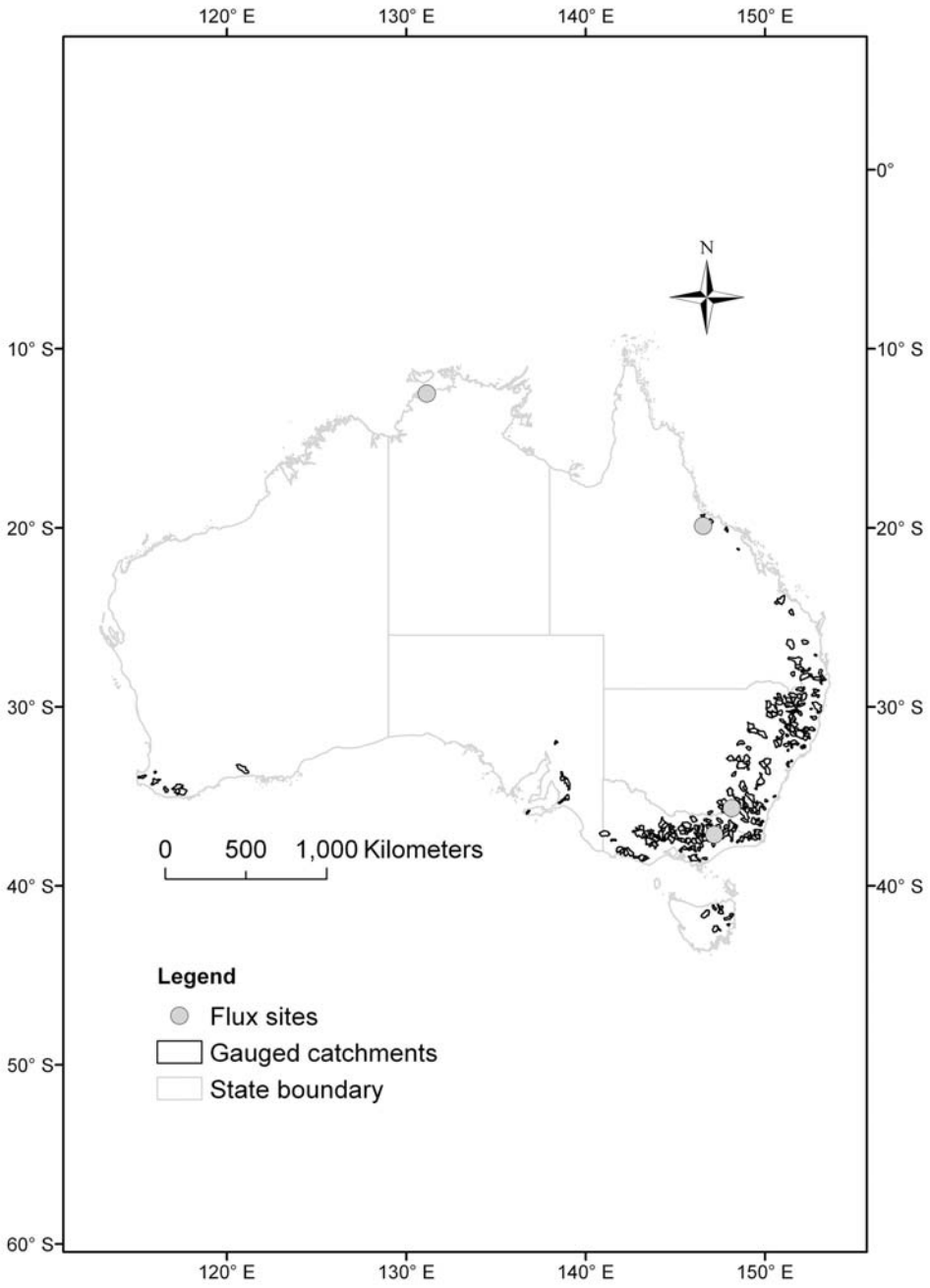

Figure 1. Location of catchments used to calibrate and validate the Fu evaporation model, four flux station flux sites, and seven soil moisture stations.

[25] Varying α by ±10% around its optimized value has only a small influence on the evaporation index (Figure 3a) but significantly affects the predicted values of $\overline{E}_{\mathrm{Fu}}$. Increasing α by 10% above its optimal value results in an RMSE of 70.9 mm/yr and an NSE = 0.76 when compared to $\overline{E}_{\mathrm{WB}}$, while a 10% decrease in α causes a further degradation on $\overline{E}_{\mathrm{Fu}}$, indicated by an RMSE of 107.9 mm/yr and an NSE = 0.45.

[26] A further analysis was conducted to determine whether varying the parameter α in equation (4) for different land cover types would improve predictions of $\overline{E}_{\mathrm{Fu}}$. We first took $\overline{E}_{\mathrm{WB}}$ for each catchment as the sum of $x_j\,\overline{E}_{\mathrm{WB},j}$, where x_j is the fractional cover and $\overline{E}_{\mathrm{WB},j}$ is the mean annual evaporation for $j = 1,\ldots, N$ land cover types (here $N = 14$ for the 13 vegetation types and 1 water body type, for which mean annual evaporation was calculated using equation (5)). A constant value (α_j) for each vegetation type was estimated by optimizing the 13-parameter Fu model using $\overline{E}_{\mathrm{WB},j}$ for all 285 gauged catchments. In a finding similar to that of *Oudin et al.* [2008], there was only a marginal improvement in model predictions of $\overline{E}_{\mathrm{Fu}}$ using 13 parameters rather than 1. The RMSE for evaporation runoff was reduced from 57.1 to 55.1 mm/yr with improvements in the NSE of <0.02. As a

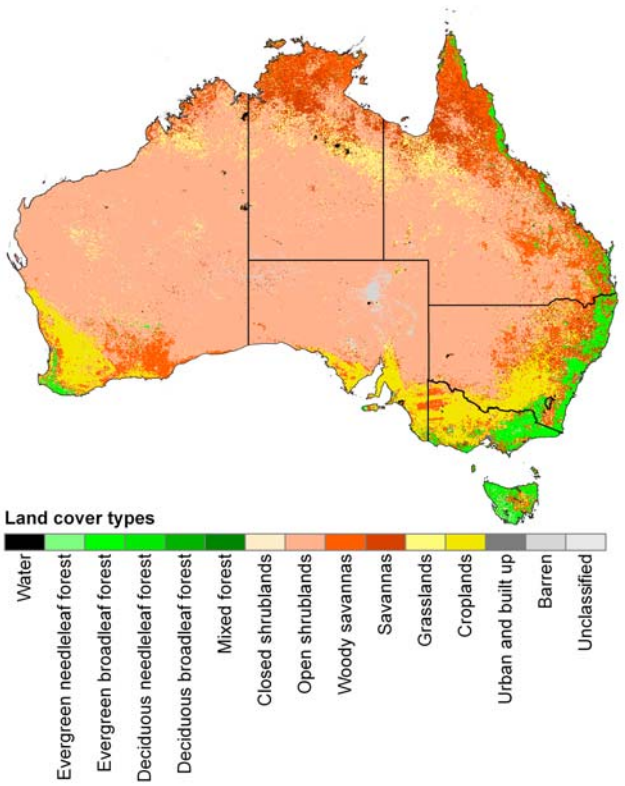

Figure 2. Land cover distribution across Australia from Moderate Resolution Imaging Spectrometer land cover classification product.

consequence of these findings, the one-parameter Fu model was used in all subsequent calculations.

5.2. Continental Long-Term Water Balance and g_{sx} Maps

[27] Figure 4a shows mean annual precipitation ($\overline{P}$) for the period 2000 to 2005 at 0.05° resolution across Australia, while Figures 4b and 4c show $\overline{E}_{\mathrm{Fu}}$ and $\overline{Q}_{\mathrm{Fu}}$ predicted using the calibrated Fu model. Note that calculating $\overline{Q}_{\mathrm{Fu}} = \overline{P} - \overline{E}_{\mathrm{Fu}}$ for each 0.05° neglects lateral flow between pixels and assumes no change in soil water storage over the averaging period. Mean annual runoff is small for Australia compared to that from other continents [*Peel et al.*, 2005]; that is, $\overline{E} \approx \overline{P}$, and hence the spatial pattern of $\overline{E}_{\mathrm{Fu}}$ is similar to that of $\overline{P}$ (compare Figures 4a and 4b). Both $\overline{E}_{\mathrm{Fu}}$ and $\overline{P}$ exhibit high values in the north, east, and southwest of Australia and in western Tasmania, and both decrease gradually from the east and north to the center of Australia. Significant quantities of runoff occur in northern and eastern Australia, Tasmania, and southwest Australia, while the other regions produce little or no runoff (Figure 4c).

[28] Figure 5 provides a map of g_{sx}, the maximum stomatal conductance parameter in the PML model. There is a high correlation ($R = 0.70$ on a cell by cell basis) between the spatial patterns of g_{sx} and mean annual precipitation, indicating the strong control of maximum stomatal conductance by precipitation in this water-limited continent. High values of g_{sx} occur in regions covered by forests, closed shrublands, and tropical savannas, while low values of g_{sx} are mainly located in the regions covered by open shrublands in central Australia.

[29] Estimates of means and standard deviations of g_{sx} for each land cover class are presented in Table 2 along with the number of grid cells allocated to each land cover class. Values of g_{sx} for most classes fall within the physiologically reasonable range of 0.003–0.01 m/s reported by *Kelliher et al.* [1995]. Note that g_{sx} for irrigated cropland is underestimated because the long-term water balance equation, ($\overline{E}_{\mathrm{WB}} = \overline{P} - \overline{Q}$), does not consider irrigation inputs for irrigated cropland. Standard deviations of g_{sx} are similar in magnitude to the means, but the corresponding standard errors are very small, given the large number of pixels in most classes.

[30] These results are encouraging, but it is important to note that g_{sx} is a parameter of the PML model estimated for each 0.05° grid cell and hence is unlikely to match stomatal conductance measurements on actual vegetation. While the optimized value of g_{sx} is constant for each pixel, canopy conductances and evaporation rates vary on time scales from minutes to years in response to variation in absorbed radiation, humidity deficit, temperature, wind speed, and LAI (equations (1)–(3)). It is acceptable to use successive 8 day LAI values from MODIS to calculate G_c (equation (3)) because seasonal variation in LAI is gradual for most vegetation. Exceptions occur during leaf emergence and leaf fall for deciduous vegetation and for rapidly growing crops. In these cases, short-term variability in LAI can be interpolated using the 8 day MODIS values.

5.3. Comparing $\overline{E}_{\mathrm{WB}}$ With $\overline{E}_{\mathrm{PML}}$ Calculated Using Alternative Estimates of g_{sx}

[31] Figure 6 compares evaporation rates ($\overline{E}_{\mathrm{WB}}$) derived from the water balances of the 285 gauged catchments with $\overline{E}_{\mathrm{PML}}$ calculated using three different approaches to estimating g_{sx} and G_x. The first uses the calibrated Fu model to calculate $\overline{E}_{\mathrm{Fu}}$ and then the value of g_{sx} needed to match $\overline{E}_{\mathrm{Fu}}$ and $\overline{E}_{\mathrm{PML}}$, as discussed above. The second uses fixed,

Table 1. Details of Flux Sites Used in This Study to Validate 8 Day Variation of Evaporation Estimated From the PM-Leuning Model[a]

Site Name	Location (Lat./Lon.) Elevation (asl)	Land Cover Type	Mean Annual Rainfall (mm)	Mean Annual Leaf Area Index	Measurement Period	Reference
Tumbarumba	−35.656° 148.152° 1200 m	Evergreen broadleaf forest	1027	2.6	Feb 2002 to Apr 2005	*Leuning et al.* [2005]
Virginia Park	−19.883° 146.554° 290 m	Open woody savanna	524	0.6	Jul 2001 to Feb 2003	*Leuning et al.* [2005]
Howard Springs	−12.495° 131.150° 37 m	Woody savanna	1764	1.4	Aug 2001 to Dec 2005	*Beringer et al.* [2003, 2007]
Dargo High Plains	−37.1333° 147.171° 1518 m	Grassland	1126	2.8	Jan 2007 to Dec 2008	-

[a]Abbreviation is as follows: asl, above sea level.

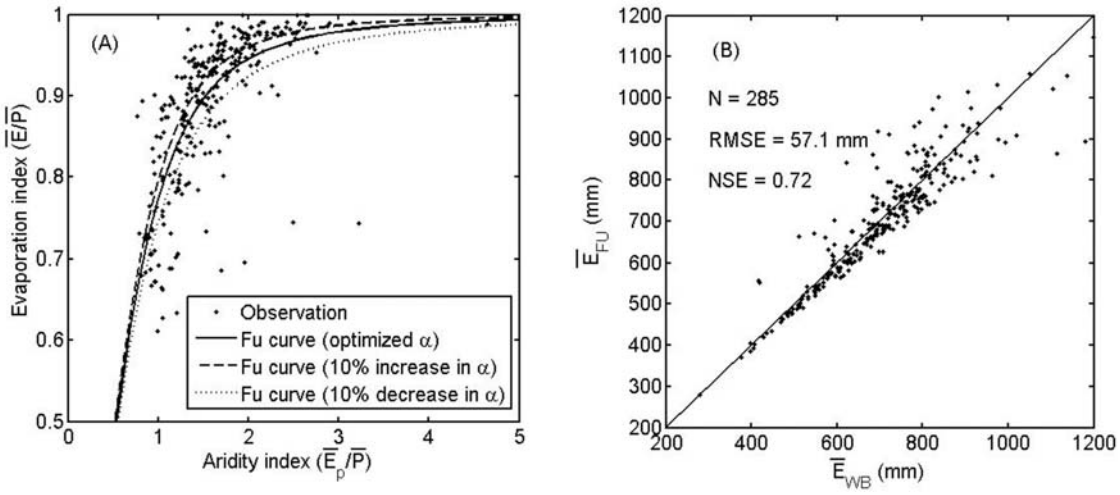

Figure 3. (a) Aridity index ($\overline{E}_p/\overline{P}$) versus evaporation index ($\overline{E}/\overline{P}$) for 285 gauged catchments by which the optimized value of α, the parameter in the Fu model (equation (4)), is 3.39. (b) Simulated mean annual evaporation ($\overline{E}_{Fu}$) from the calibrated Fu model versus estimates from catchment water balances ($\overline{E}_{WB} = \overline{P} - \overline{Q}_{obs}$). Each point presents one catchment. RMSE is the root-mean square error, and NSE is the Nash-Sutcliffe efficiency across 285 catchments.

optimized values of g_{sx} and f for each of several "super-classes" of vegetation obtained by *Leuning et al.* [2008] using measurements of daily latent heat fluxes at 15 sites across the globe. Value of g_{sx} and f for vegetation classes in each gauged catchment were assigned according to their nearest superclass. Third, following *Zhang et al.* [2008], the catchments were divided into three rainfall zones (P_1 > 750 mm/yr, 450 ≤ P_2 ≤ 750 mm/yr, and P_3 < 450 mm/yr) to estimate optimized values of g_{sx} and f in each zone. Values of g_{sx} and f were then assigned for each rainfall zone across Australia.

[32] There is good agreement between $\overline{E}_{WB}$ and $\overline{E}_{PML}$ derived using the Fu model to estimate g_{sx}, as indicated by an RMSE of 58.3 mm/yr and NSE = 0.84 (Figure 6a). The corresponding comparison between the observed runoff $\overline{Q}_{obs}$ and $\overline{Q}_{PML} = \overline{P} - \overline{E}_{PML}$ yields RMSE = 58.3 mm/yr and NSE = 0.70 (Figure 6b). Using vegetation classes to assign values of g_{sx} and f considerably reduces model performance, increasing the RMSE to 119.8 mm/yr for evaporation and to 97.7 mm/yr for runoff, after setting $\overline{Q}_{PML}$ = 0 mm/yr for the 30% of catchments where $\overline{E}_{PML}$ is > $\overline{E}_{WB}$ (Figure 6c and 6d). Relatively poor results for both $\overline{E}_{PML}$ and $\overline{Q}_{PML}$ are also obtained when g_{sx} and f are assigned to one of three rainfall zones (Figures 6e and 6f). Using a water balance model to constrain parameters values in the PML energy balance model clearly yields superior results to those obtained by assigning values of g_{sx} and f using either the vegetation superclass or rainfall zone. In both of these schemes there was no constraint by the water balance on the optimized parameter values.

5.4. Performance of the 8 Day E_{PML}

[33] The previous results compared mean annual evaporation and runoff. The PML model is not really needed at the annual time scale, but it is useful for estimating evaporation rates at much smaller time scales. In this section, we evaluate performance of the PML model by comparing 8 day average E_{PML} with corresponding evaporation fluxes (E_{meas}) measured at the four Australian flux station sites where data were available for more than 1 year (Figure 1). E_{PML} is calculated using g_{sx} calibrated using the Fu model for the grid cell containing each flux station. Figure 7 shows that z reproduces the seasonal variation in E_{meas} quite well at Tumbarumba and to a lesser degree at Virginia Park. *Leuning et al.* [2008] obtained an RMSE of 0.54 mm/d at Tumbarumba and an RMSE of 0.57 mm/d at Virginia Park in scatterplots of E_{PML} versus E_{meas} when g_{sx} was calibrated using local flux data. In contrast, using estimates of g_{sx} from the Fu model gave poorer results at Tumbarumba, indicated by an RSME of 0.99 mm/d, but with little difference at Virginia Park (RMSE of 0.56 mm/d, Figure 7). The slope of the linear regression for the Tumbarumba data was 1.20, which is significantly greater than unity. This result is likely due to a mismatch between the spatial and temporal scales of the flux measurements and the Fu model or because MODIS LAI is overestimated at this site [*Leuning et al.*, 2005]. The slope of the linear regression of E_{PML} versus E_{meas} for the Virginia Park data is 0.70, but the large scatter in the data indicates that this is not significantly different from unity.

[34] Seasonal variation in evaporation at Howard Springs is also simulated well, with scatterplots of E_{PML} versus E_{meas} having an RMSE of 1.13 mm/d and R^2 = 0.53 (Figure 7). The time series shows that the PML model overestimated E by ~1 mm/d in the dry seasons of 2001 and 2004, but there was good agreement between model and measurements for the other three dry seasons. These results are encouraging because the model is able to account for variation in E caused by the strong seasonal variation in climate and the dramatic changes in LAI due to a mixture of C_3 trees and C_4 grasses in the wet season and trees only in the dry season [*Grady et al.*, 2000].

[35] In contrast, E_{PML} is systematically greater than the eddy flux measurements at Dargo High Plains (Figure 7). The scatterplot has a slope of 1.58, an RMSE of 1.56 mm/d, and R^2 = 0.65. To investigate the reason of overestimation, we checked the energy balance closure between $R_n - G$ and

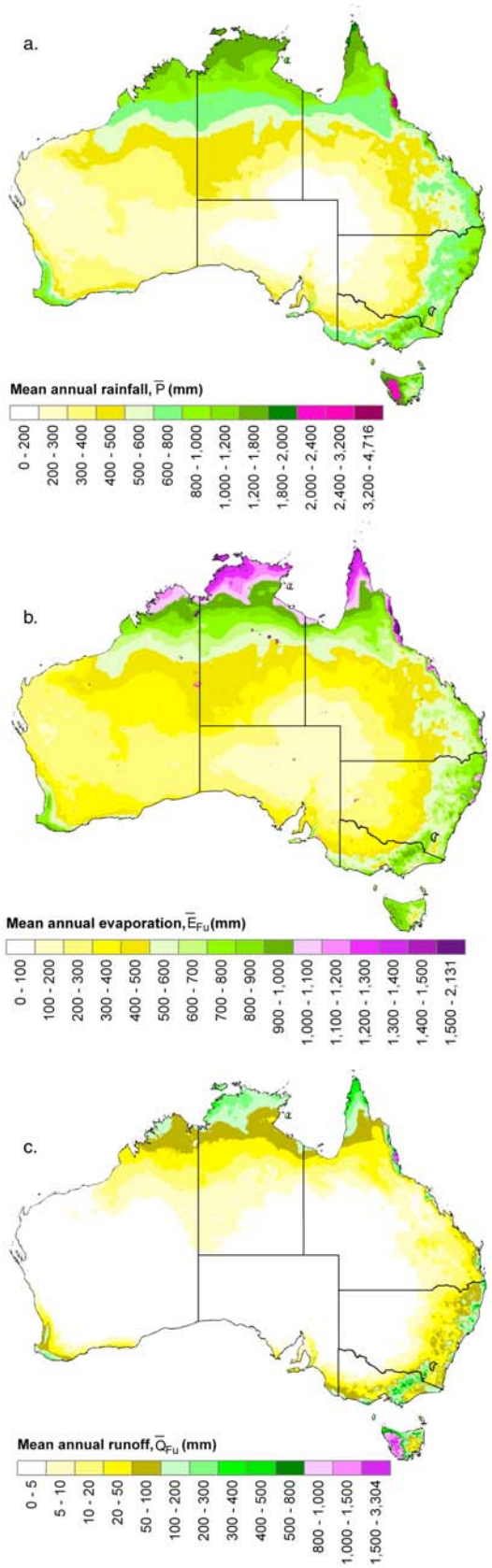

Figure 4. Spatial pattern in mean annual (a) precipitation ($\overline{P}$), (b) evaporation ($\overline{E}_{Fu}$), and (c) runoff ($\overline{Q}_{Fu}$) across Australia. $\overline{E}_{Fu}$ and $\overline{Q}_{Fu}$ are predicted using the calibrated Fu model.

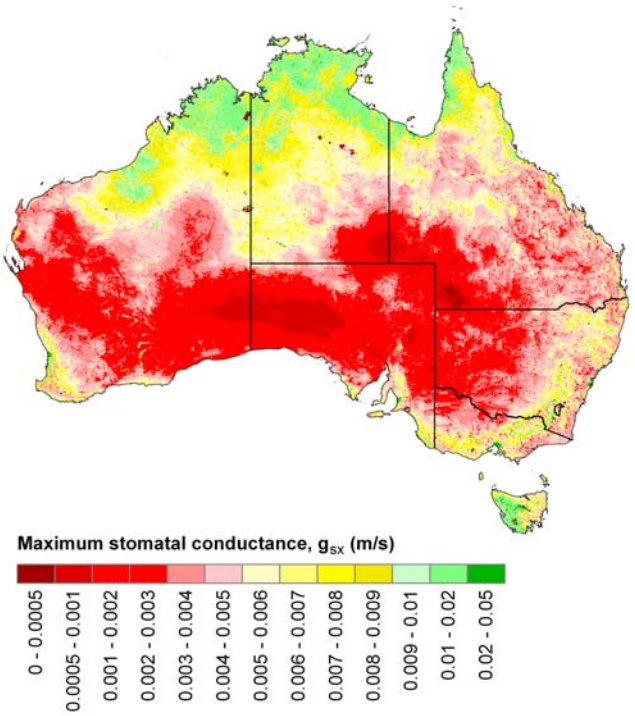

Figure 5. Spatial pattern in the maximum stomatal conductance parameter (g_{sx}) across Australia.

$\lambda E + H$ at the four sites, where R_n, G, λE, and H are the measured net radiation, soil heat flux, latent heat flux, and sensible heat flux, respectively.

[36] Figure 8 shows that the linear regression slopes are close to unity at Tumbarumba, Virginia Park, and Howard Springs, but that there is relatively poor energy balance closure at Dargo High Plains, where the slope of $\lambda E + H$ versus $R_n - G$ is only 0.80. This result suggests that the measured latent heat flux is underestimated at that site and may explain the apparent overestimation of E_{meas} by E_{PML} at Dargo High Plains.

[37] The results in Figure 7 are for the pixels in which each of the flux stations are located, and while these comparisons between model and measurements are encouraging, the question of the representativeness of flux stations often arises. To analyze the model uncertainty due to pixel

Table 2. Statistical Analysis of Maximum Stomatal Conductance Estimated From the Fu Model for Each Land Cover Type

Land Cover Types	g_{sx} (m/s) Mean (SD)	Pixels	
		Number	Percent
Evergreen needleleaf forest	0.0086 (0.0104)	1,563	0.56
Evergreen broadleaf forest	0.0063 (0.0059)	10,477	3.76
Deciduous needleleaf forest	0.0059 (0.0090)	42	0.02
Deciduous broadleaf forest	0.0081 (0.0069)	774	0.28
Mixed forest	0.01 (0.0115)	405	0.15
Closed shrublands	0.0067 (0.0071)	1,359	0.49
Open shrublands	0.0042 (0.0029)	183,476	65.77
Woody savannas	0.0059 (0.0048)	23,932	8.58
Savannas	0.0071 (0.0045)	19,997	7.17
Grasslands	0.0059 (0.0039)	15,181	5.44
Croplands	0.0048 (0.0023)	172,710	6.19
Urban and built up	0.0199 (0.0179)	322	0.12
Barren and unclassified	0.0034 (0.0028)	4,174	1.50

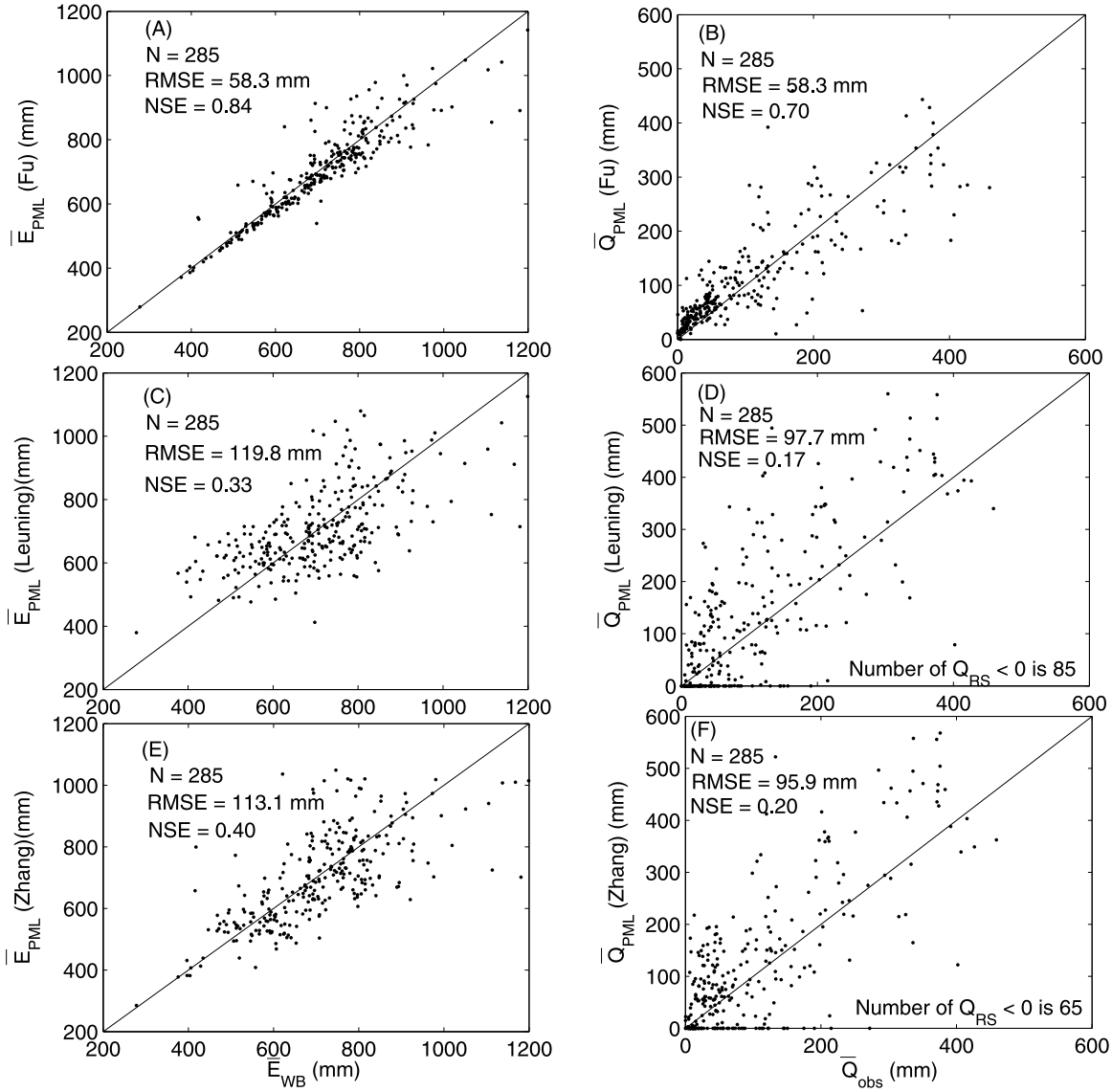

Figure 6. Simulated mean annual (a) evaporation (E_{PML}) and (b) runoff ($\overline{Q}_{PML} = \overline{P} - \overline{E}_{PML}$) calculated using the PML model with g_{sx} estimated from the Fu model, (c, d) those obtained using g_{sx} allocated according to vegetation superclasses, and (e, f) those obtained using the optimized g_{sx} and f parameters in three climatic zones, plotted against evaporation estimates from catchment water balances ($\overline{E}_{WB} = \overline{P} - \overline{Q}_{obs}$).

selection, the RMSE between flux measurements and E_{PML} for the eight pixels surrounding a given flux tower are shown in Figure 9. The average RMSE values are 0.94, 0.53, 1.17, and 1.26 mm/d for Tumbarumba, Virginia Park, Howard Springs, and Dargo High Plains, respectively. The standard deviation in RMSE for Dargo High Plains is 0.23 mm/d and is <0.10 mm/d for other three sites, indicating strong homogeneity in E_{PML} for the pixels surrounding each flux station.

[38] While four flux stations cannot be representative of the Australian continent, Virginia Park and Howard Springs are located in savannas, the second largest land cover type, occupying 15.7% of Australia. Grasslands (Dargo High Plains) and evergreen broadleaf forest (Tumbarumba) account for 5.44% and 3.76%, respectively. However, for a comprehensive evaluation of the PML model, more validation needs to be done at other biomes, such as open shrubs and croplands, which are widely distributed in Australia.

[39] In Figure 6 we showed that using either vegetation superclasses or rainfall zones to assign g_{sx} and f to calculate $\overline{E}_{PML}$ gave significantly worse results than when g_{sx} was constrained using the Fu model. Comparison of Figures 7 and 10 shows that similar conclusions apply when rainfall zones are used to assign g_{sx} and f to estimate 8 day evaporation rates. These estimates of E_{PML} are worse than those obtained using variable f and the Fu model to estimated g_{sx} at Virginia Park and Howard Springs, but not for Tumbarumba and Dargo High Plains. Varying f at Virginia Park and Howard Springs improves model performance compared to using a fixed value of f because both these savanna sites have low LAI compared to Tumbarumba, which is a broadleaf forest, and Dargo High Plains, which is a grassland (Table 1). A sensitivity analysis by *Leuning et al.*

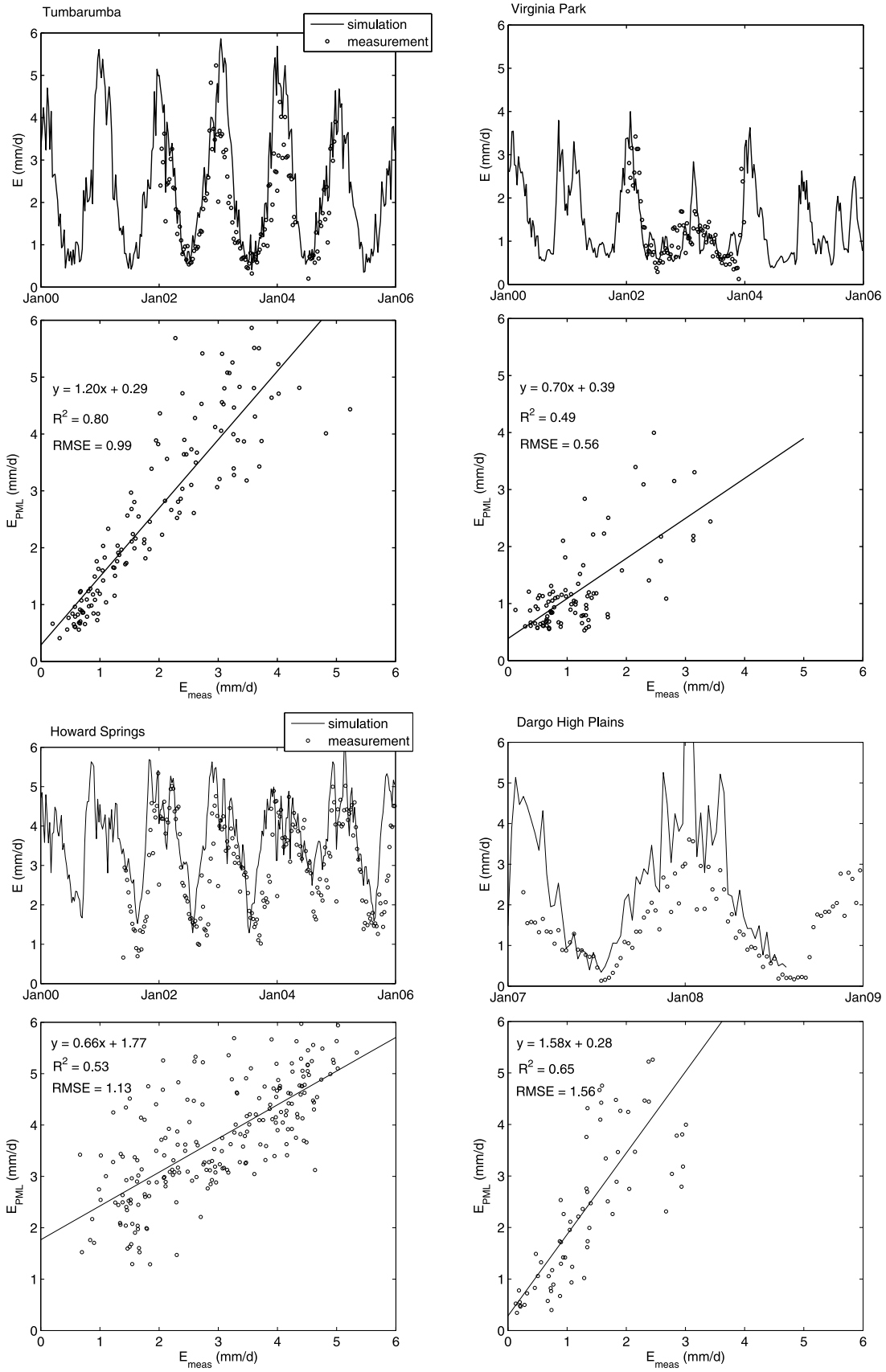

Figure 7. (top) Time series of 8 day averages for E_{meas} and E_{PML} obtained using the variable f and g_{sx} estimated with the Fu model and (bottom) scatterplots of E_{PML} versus E_{meas} at four flux sites, Tumbarumba, Virginia Park, Howard Springs, and Dargo High Plains.

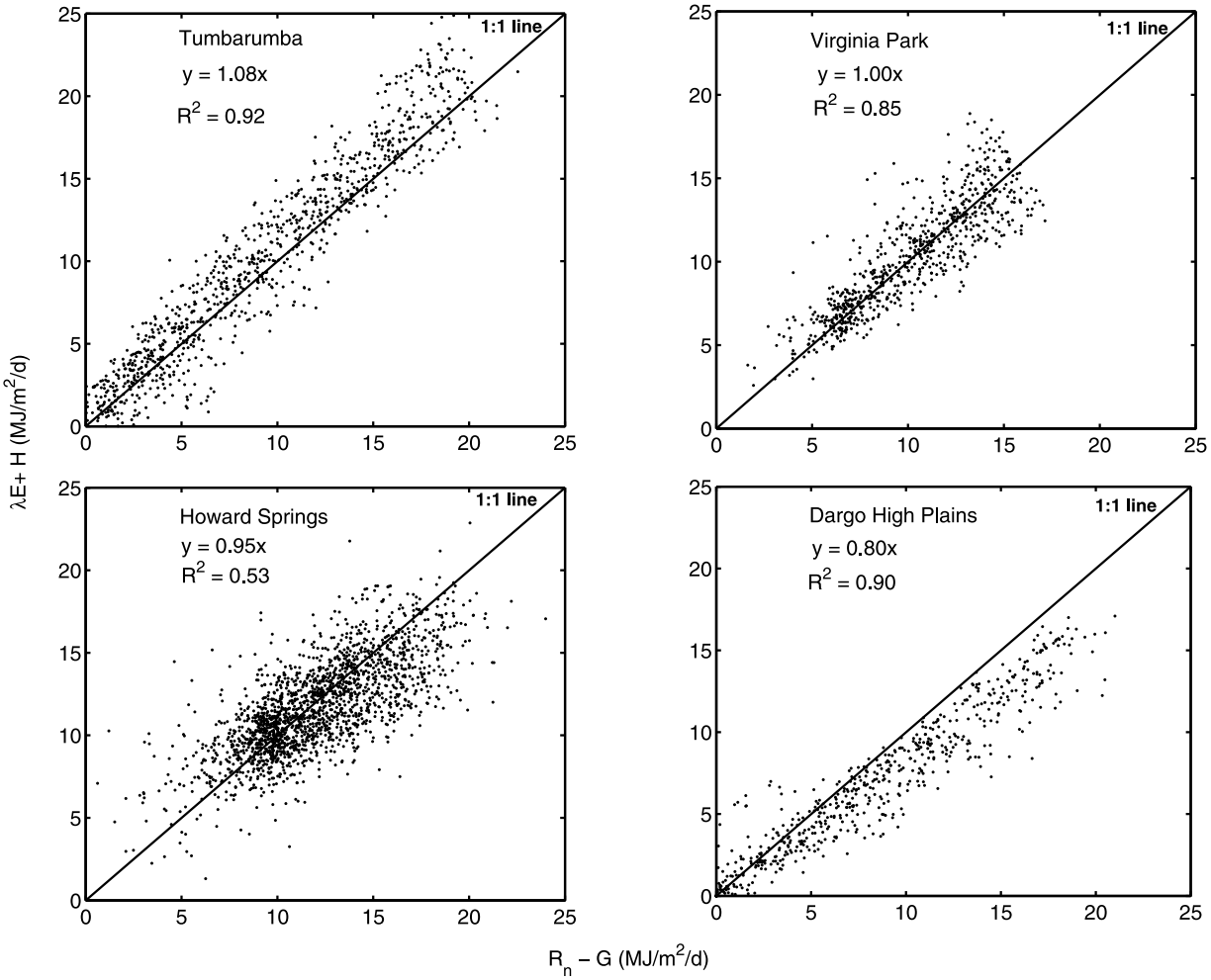

Figure 8. Scatterplots of measured daily average $\lambda E + H$ versus daily average available energy $A = R_n - G$ for each of four selected flux sites. Slopes and R^2 values are shown for linear regressions forced through the origin.

[2008] found that the PML model is highly sensitive to variation in f for LAI < 2.5, when evaporation from moist soil will account for a large fraction of the total evaporation. In contrast, the PML model is not sensitive to the variation in f when LAI > 2.5. Hence, it is essential that f be treated as a variable rather than as a constant for vegetation with low LAI.

[40] This paper presents an advance on the work of *Cleugh et al.* [2007], who estimated surface conductance simply as LAI multiplied by a constant while neglecting evaporation from the soil surface. By allowing the soil evaporation parameter f to vary within each 8 day period, this paper is also an improvement on the work of *Leuning et al.* [2008], who calibrated the PML model for 15 flux stations distributed globally while holding f constant for each site. *Zhang et al.* [2008] also used water balances of unregulated catchments to calibrate g_{sx} and f to estimate evaporation and runoff using the PML model for the two broad climate zones across the Murray-Darling Basin of Australia. However, their calibration approach did not constrain the annual evaporation rate to be less than or equal to annual precipitation, potentially leading to negative values of runoff. The present study overcomes this problem

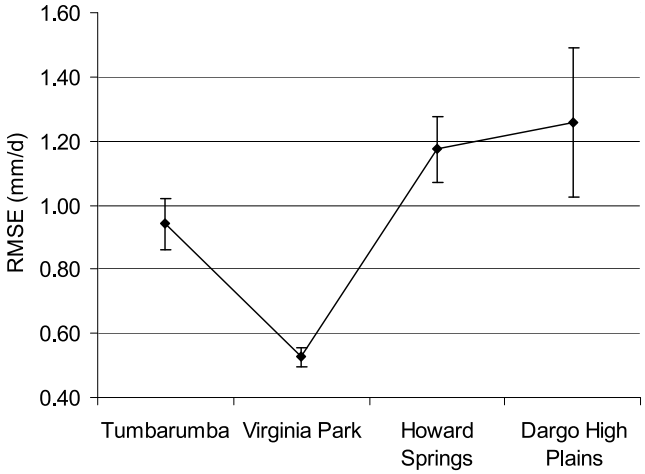

Figure 9. Mean (dots) and standard deviation (error bars) of the root mean square errors obtained by comparing measured fluxes to E_{PML} for each of the eight pixels surrounding a flux tower.

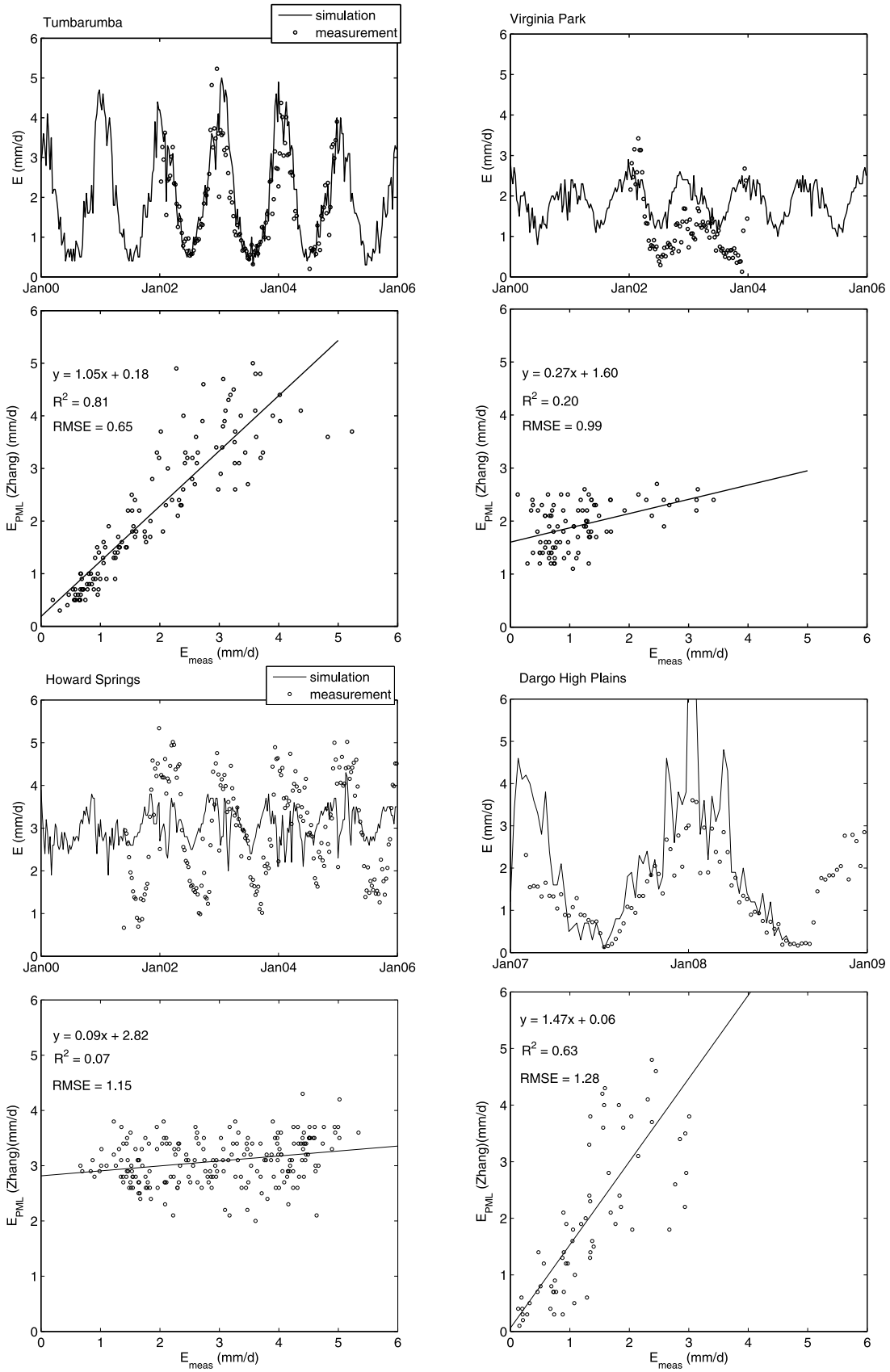

Figure 10. As for Figure 7, but using optimized values of g_{sx} and f in three climatic regimes.

by optimizing the value of g_{sx} for each pixel to ensure that annual evaporation from the Fu water balance model is equal to that from PML energy balance model.

[41] The results in Figures 6a, 6b, and 7 provide confidence in our use of equation (2) to estimate the spatial and temporal variation in f and the Fu catchment water balance model to estimate the spatial distribution of g_{sx}. The calibrated PML model provides estimates of evaporation at weekly to annual time scales for each 0.05° grid cell using gridded meteorological fields and remotely sensed leaf area indices, albedos, and land cover classes. Such high temporal resolution of evaporation is not possible with the Budyko mean annual water balance approaches.

[42] A further advantage is that estimates of short-term E_{PML} can also be used to calibrate catchment-scale, daily hydrological models. Using cross validation, *Zhang et al.* [2009] showed that a rainfall-runoff model calibrated using E_{PML} and daily streamflow data significantly improved estimates of the daily to monthly runoff from ungauged catchments compared to using only streamflow data to calibrate the model.

[43] Having presented a method for estimating the spatial distribution of a key model parameter for the PML model of evaporation from landscapes, there remains the challenge of testing model performance at multiple space and time scales. This can be achieved by comparison with data from additional flux stations and using runoff from uncalibrated catchments.

6. Conclusion

[44] This paper applies the Penman-Monteith-Leuning energy balance model to estimate evaporation from vegetation and the soil at 0.05° spatial resolution and at 8 day time scales. The PML model uses remotely sensed leaf area indices, land cover type, and gridded meteorological fields and requires two parameters, f and g_{sx}, to account for soil evaporation and plant transpiration, respectively. Previously treated as a constant, f in this paper is now a variable dependent on precipitation and equilibrium evaporation at the soil surface. The spatial distribution of g_{sx} was obtained by optimizing the value of g_{sx} for each grid cell to ensure that annual water balances calculated using the PML model equaled those from the Fu hydrometeorological model. The Fu model was calibrated using long-term precipitation and runoff data from 285 unregulated, gauged catchments, and then the calibrated Fu model was used to estimate the spatial distribution of mean annual evaporation across Australia. Satisfactory agreement was obtained between 8 day evaporation rates from the PML model and measurements at four flux stations. There was also excellent agreement between mean annual evaporation from catchment water balances and the PML model.

[45] **Acknowledgments.** The study was supported by the water information research and development alliance between Commonwealth Scientific and Industrial Research Organization (CSIRO) and the Australian Bureau of Meteorology. We are grateful to Edward King for providing the mosaic MODIS LAI data set used in this study. Special thanks are extended to Albert Van Dijk and Juan Pablo Guerschman (both from CSIRO Land and Water) and three anonymous reviewers for their constructive comments on this paper.

References

Beringer, J., L. B. Hutley, N. J. Tapper, A. Coutts, A. Kerley, and A. P. O'Grady (2003), Fire impacts on surface heat, moisture and carbon fluxes from a tropical savanna in northern Australia, *Int. J. Wildland Fire*, *12*, 333–340, doi:10.1071/WF03023.

Beringer, J., L. B. Hutley, N. J. Tapper, and L. A. Cernusak (2007), Savanna fires and their impact on net ecosystem productivity in North Australia, *Global Change Biol.*, *13*, 990–1004, doi:10.1111/j.1365-2486.2007.01334.x.

Budyko, M. I. (1958), *The Heat Balance of the Earth's Surface*, U.S. Dep. of Commerce, Washington, D. C.

Budyko, M. I. (1974), *Climate and Life*, Academic, San Diego, Calif.

Cleugh, H. A., R. Leuning, Q. Z. Mu, and S. W. Running (2007), Regional evaporation estimates from flux tower and MODIS satellite data, *Remote Sens. Environ.*, *106*, 285–304, doi:10.1016/j.rse.2006.07.007.

Cohen, W. B., T. K. Maiersperger, D. P. Turner, W. D. Ritts, D. Pflugmacher, R. E. Kennedy, A. Kirschbaum, S. W. Running, M. Costa, and S. T. Gower (2006), MODIS land cover and LAI collection 4 product quality across nine sites in the Western Hemisphere, *IEEE Trans. Geosci. Remote Sens.*, *44*, 1843–1857, doi:10.1109/TGRS.2006.876026.

Dilley, A. C., M. Edwards, D. M. O'Brien, and R. M. Mitchell (2000), Operational AVHRR processing modules: Atmospheric correction, cloud masking and BRDF compensation, *Paper 14, EOC Project Final Rep.*, 24 pp., CSIRO Div. of Atmos. Res., Victoria, Australia.

Dolman, A. J., J. H. C. Gash, J. Roberts, and W. J. Shuttleworth (1991), Stomatal and surface conductance of tropical rain-forest, *Agric. Forest Meteorol.*, *54*, 303–318, doi:10.1016/0168-1923(91)90011-E.

Fu, B. P. (1981), On the calculation of the evaporation from land surface (in Chinese), *Sci. Atmos. Sin.*, *5*, 23–31.

Garrigues, S., et al. (2008), Validation and intercomparison of global leaf area index products derived from remote sensing data, *J. Geophys. Res.*, *113*, G02028, doi:10.1029/2007JG000635.

Grady, A. P. O., X. Chen, D. Eamus, and L. B. Hutley (2000), Composition, leaf area index and standing biomass of eucalypt open forests near Darwin in the Northern Territory, Australia, *Aust. J. Bot.*, *48*, 629–638, doi:10.1071/BT99022.

Hill, M. J., U. Senarath, A. Lee, M. Zeppel, J. M. Nightingale, R. D. J. Williams, and T. R. McVicar (2006), Assessment of the MODIS LAI product for Australian ecosystems, *Remote Sens. Environ.*, *101*, 495–518, doi:10.1016/j.rse.2006.01.010.

Hutchinson, M. F., J. A. Stein, and J. L. Stein (2001), Upgrade of the 9 second digital elevation model for Australia, Cent. for Resour. and Environ. Studies Aust. Natl, Univ., Canberra, Australia.

Isaac, P. R., R. Leuning, J. M. Hacker, H. A. Cleugh, P. A. Coppin, O. T. Denmead, and M. R. Raupach (2004), Estimation of regional evapotranspiration by combining aircraft and ground-based measurements, *Boundary Layer Meteorol.*, *110*, 69–98, doi:10.1023/A:1026054317990.

Jeffrey, S. J., J. O. Carter, K. B. Moodie, and A. R. Beswick (2001), Using spatial interpolation to construct a comprehensive archive of Australian climate data, *Environ. Model. Software*, *16*, 309–330, doi:10.1016/S1364-8152(01)00008-1.

Jonsson, P., and L. Eklundh (2004), TIMESAT: A program for analyzing time-series of satellite sensor data, *Comput. Geosci.*, *30*, 833–845, doi:10.1016/j.cageo.2004.05.006.

Kelliher, F. M., R. Leuning, M. R. Raupach, and E. D. Schulze (1995), Maximum conductances for evaporation from global vegetation types, *Agric. Forest Meteorol.*, *73*, 1–16, doi:10.1016/0168-1923(94)02178-M.

Leuning, R., H. A. Cleugh, S. J. Zegelin, and D. Hughes (2005), Carbon and water fluxes over a temperate eucalyptus forest and a tropical wet/dry savanna in Australia: Measurements and comparison with MODIS remote sensing estimates, *Agric. Forest Meteorol.*, *129*, 151–173, doi:10.1016/j.agrformet.2004.12.004.

Leuning, R., Y. Q. Zhang, A. Rajaud, and H. A. Cleugh (2008), A simple surface conductance model to estimate evaporation using MODIS leaf area index and the Penman-Monteith equation, *Water Resour. Res.*, *44*, W10419, doi:10.1029/2007WR006562.

McVicar, T. R., T. G. Van Niel, L. T. Li, M. L. Roderick, D. P. Rayner, L. Ricciardulli, and R. J. Donohue (2008), Wind speed climatology and trends for Australia, 1975–2006: Capturing the stilling phenomenon and comparison with near-surface reanalysis output, *Geophys. Res. Lett.*, *35*, L20403 doi:10.1029/2008GL035627.

Monteith, J. L. (1964), Evaporation and environment. The state and movement of water in living organisms, in *Symposium of the Society of Experimental Biology*, vol. 19, edited by G. E. Fogg, pp. 205–234, Academic, New York.

Mu, Q. Z., F. A. Heinsch, M. S. Zhao, and S. W. Running (2007), Development of a global evapotranspiration algorithm based on MODIS and global meteorology data, *Remote Sens. Environ.*, *111*, 519–536, doi:10.1016/j.rse.2007.1004.1015.

Myneni, R. B., et al. (2002), Global products of vegetation leaf area and fraction absorbed PAR from year one of MODIS data, *Remote Sens. Environ.*, *83*, 214–231, doi:10.1016/S0034–4257(02)00074–3.

Nash, J. E., and J. V. Sutcliffe (1970), River forecasting using conceptual models: 1. A discussion of principles, *J. Hydrol. Amsterdam*, *10*, 280–290.

Oudin, L., V. Andreassian, J. Lerat, and C. Michel (2008), Has land cover a significant impact on mean annual streamflow? An international assessment using 1508 catchments, *J. Hydrol. Amsterdam*, *357*, 303–316, doi:10.1016/j.jhydrol.2008.05.021.

Paget, M. J., and E. A. King (2008), MODIS Land data sets for the Australian region, *Internal Rep. 004*, 96 pp., CSIRO Marine and Atmos. Res., Canberra, Australia.

Peel, M. C., T. A. McMahon, and G. G. S. Pegram (2005), Global analysis of runs of annual precipitation and runoff equal to or below the median: Run magnitude and severity, *Int. J. Climatol.*, *25*, 549–568, doi:10.1002/joc.1147.

Priestley, C. H. B., and R. J. Taylor (1972), On the assessment of surface heat flux and evaporation using large-scale parameters, *Mon. Weather Rev.*, *100*, 81–92, doi:10.1175/1520-0493(1972)100<0081:OTAOSH>2.3.CO;2.

Ruffin, C., R. L. King, and N. H. Younani (2008), A combined derivative spectroscopy and Savitzky-Golay filtering method for the analysis of hyperspectral data, *Geosci. Remote Sens.*, *45*, 1–15, doi:10.2747/1548-1603.45.1.1.

Saugier, B., and N. Katerji (1991), Some plant factors controlling evapotranspiration, *Agric. Forest Meteorol.*, *54*, 263–277, doi:10.1016/0168-1923(91)90009-F.

Schaaf, C. B., et al. (2002), First operational BRDF, albedo nadir reflectance products from MODIS, *Remote Sens. Environ.*, *83*, 135–148, doi:10.1016/S0034-4257(02)00091-3.

Tsai, F., and W. Philpot (1998), Derivative analysis of hyperspectral data, *Remote Sens. Environ.*, *66*, 41–51, doi:10.1016/S0034-4257(98)00032-7.

Yang, W., N. V. Shabanov, D. Huang, W. Wang, R. E. Dickinson, R. R. Nemani, Y. Knyazikhin, and R. B. Myneni (2006), Analysis of leaf area index products from combination of MODIS Terra and Aqua data, *Remote Sens. Environ.*, *104*, 297–312, doi:10.1016/j.rse.2006.04.016.

Zhang, Y. Q., and M. Wegehenkel (2006), Integration of MODIS data into a simple model for the spatial distributed simulation of soil water content and evapotranspiration, *Remote Sens. Environ.*, *104*, 393–408, doi:10.1016/j.rse.2006.05.011.

Zhang, Y. Q., F. H. S. Chiew, L. Zhang, R. Leuning, and H. A. Cleugh (2008), Estimating catchment evaporation and runoff using MODIS leaf area index and the Penman-Monteith equation, *Water Resour. Res.*, *44*, W10420, doi:10.1029/2007WR006563.

Zhang, Y. Q., F. H. S. Chiew, L. Zhang, and H. X. Li (2009), Use of remotely sensed actual evapotranspiration to improve rainfall-runoff modeling in Southeast Australia, *J. Hydrometeorol.*, *10*, 969–980, doi:10.1175/2009JHM1061.1.

J. Beringer and I. McHugh, School of Geography and Environmental Science, Monash University, Clayton, Vic 3800, Australia.

L. B. Hutley, School of Environmental and Life Sciences, Charles Darwin University, Darwin, NT 0909, Australia.

R. Leuning, CSIRO Marine and Atmospheric Research, Canberra, ACT 2601, Australia.

J. P. Walker, Department of Civil and Environmental Engineering, University of Melbourne, Melbourne, Vic 3010, Australia.

Y. Zhang (corresponding author), CSIRO Water for a Healthy Country National Research Flagship, CSIRO Land and Water, Canberra, ACT 2601, Australia. (yongqiang.zhang@csiro)